NANO LETTERS

pubs.acs.org/NanoLett Letter

Deterministic Magnetization Switching via Tunable Noncollinear Spin Configurations in Canted Magnets

Pengwei Dou,[†] Jingyan Zhang,*[,†] Yaqin Guo, Tao Zhu, Jia Luo, Guoping Zhao, He Huang, Guoqiang Yu, Yunchi Zhao, Jie Qi, Xiao Deng, Yuanbo Wang, Jialiang Li, Jianxin Shen, Xinqi Zheng, Yanfei Wu, Hongxin Yang, Baogen Shen, and Shouguo Wang*

Cite This: *Nano Lett.* 2023, 23, 6449−6457 Read Online

ACCESS | Metrics & More | Article Recommendations | Supporting Information

ABSTRACT: Spin obit torque (SOT) driven magnetization switching has been used widely for encoding consumption-efficient memory and logic. However, symmetry breaking under a magnetic field is required to realize the deterministic switching in synthetic antiferromagnets with perpendicular magnetic anisotropy (PMA), which limits their potential applications. Herein, we report all electric-controlled magnetization switching in the antiferromagnetic Co/Ir/Co trilayers with vertical magnetic imbalance. Besides, the switching polarity could be reversed by optimizing the Ir thickness. By using the polarized neutron reflection (PNR) measurements, the canted noncollinear spin configuration was observed in Co/Ir/Co trilayers, which results from the competition of magnetic inhomogeneity. In addition, the asymmetric domain walls demonstrated by micromagnetic simulations result from introducing imbalance magnetism, leading to the deterministic magnetization switching in Co/Ir/Co trilayers. Our findings highlight a promising route to electric-controlled magnetism via tunable spin configuration, improve our understanding of physical mechanisms, and significantly promote industrial applications in spintronic devices.

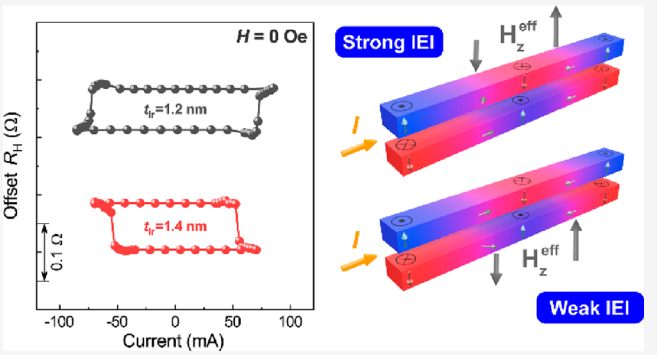

KEYWORDS: *spin−orbit torque, noncollinear spin configurations, canted magnets, asymmetric domain walls*

Spin orbit torque (SOT), due to its advantages of having low energy consumption and being nonvolatile, has emerged as a promising means of spin manipulation and attracted wide interest in information storage and neuro-computing.[1−10] Generally, the magnetization state can be triggered by the SOT, which mainly includes damping-like torque and field-like torque.[11,12] However, an in-plane-assisted magnetic field is necessary to realize field-free magnetization switching. So far, several promising approaches, mainly including structural asymmetry,[13−15] inhomogeneity film,[16−18] and internal effective field,[19−21] have been explored to achieve deterministic magnetic switching in heavy metal/ferromagnet bilayers. In addition, deterministic magnetization switching could be achieved in two-dimensional ferromagnets, which broaden the field of spintronics device.[22−24] Moreover, research on SOT-based spintronics has also been extended to both ferrimagnets (FiMs) and antiferromagnets (AFMs), owing to the advantages of ultrafast domain dynamics and suppression of stray fields.[25−33] Nevertheless, the difficulty in detecting domain information and magnetoelectric signals remains challenging owing to the fully compensated magnetizations, limiting further development of antiferromagnetic spintronics.[34−39] As promising candidates, synthetic antiferromagnets (SAFs) exhibit potential competitiveness, balancing the characteristics of negligible stray fields from AFMs, as well as easy controllability from ferromagnets.[40,41] For the perpendicular SAFs with collinear spin alignments, deterministic magnetization switching could not be achieved. Currently, field-free magnetization switching could be significantly realized when the in-plane single layer or SAFs structure was introduced to reduce symmetry.[42−44] Unfortunately, the stray fields in such SAFs, namely T-type or double SAFs, cannot be neglected, making difficult for high-density storage. To overcome the bottleneck, we propose a controllable noncollinear canted spin configuration to realize all-electric-control magnetization switching. Furthermore, the titling angles should be tuned by the competition with various energy barriers, such as perpendicular magnetic anisotropy (PMA), interlayer

Received: April 5, 2023
Revised: June 26, 2023
Published: June 28, 2023

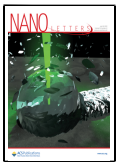

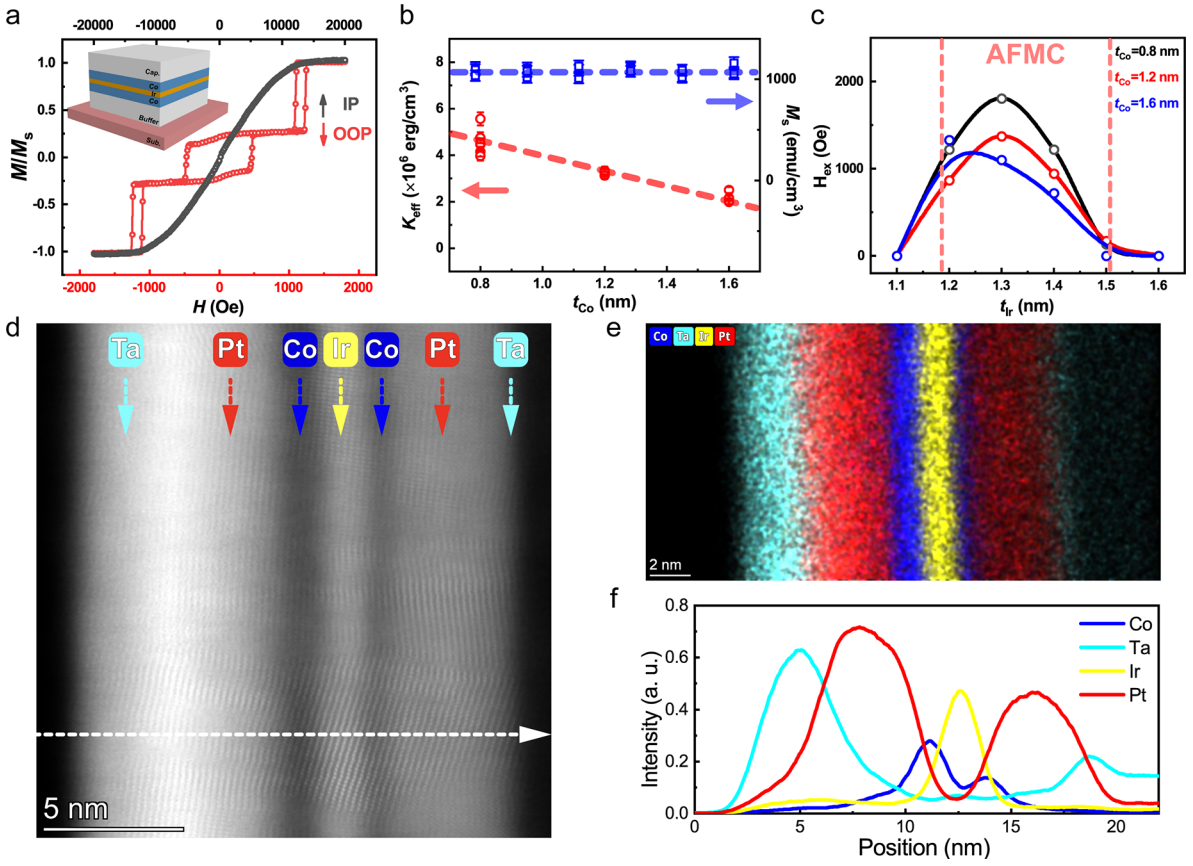

Figure 1. (a) Magnetic hysteresis ($M-H$) loops for Co(0.8)/Ir(1.2)/Co(0.8) (in nm) trilayers under vertical and in-plane magnetic fields. Inset, the schematic setup of the multilayers. (b) The effective magnetic anisotropy (K_{eff}) and saturation magnetization (M_s) as functions of bottom Co layer thickness (t_{Co}) in Co(t_{Co})/Ir/Co(0.8) trilayers (in nm). (c) The exchange coupling field (H_{ex}) as a function of t_{Ir} for the trilayers with various t_{Co}. (d) High-resolution HAADF-STEM image of Co(1.6)/Ir(1.4)/Co(0.8) (in nm). The white dotted line is the line scanning direction of EDS. (e) Ta L_α edge, Pt L_α edge, Co K_α edge, and Ir L_α edge EDS mappings. (f) The element scanning along the normal direction of the film.

exchange interaction (IEI), Dzyaloshinskii-Moriya interaction (DMI) and so on. In the study, polarized neutron reflection was used to characterize the noncollinear canted spin texture in out-of-plane magnetized Co/Ir/Co trilayers. Field-free magnetization switching could be successfully achieved by optimizing the canted spin textures. In addition, the noncollinear spin configuration can be effectively tuned by varying the thickness of the Ir spacer, enabling the reversal of the current-driven magnetization switching polarity. Furthermore, micromagnetic simulations show the mixed domain wall between Bloch and Néel type induced by the magnetic inhomogeneity results in the asymmetric domain walls breaking symmetry, leading to deterministic magnetization switching without any assistant fields. This observation represents an effective approach toward the utilization of SAFs as a core stack of SOT-based logic-in-memory.

Co/Ir/Co trilayers is a typical SAFs, in which both the topological magnetism and SOT driven magnetization switching under assistance magnetic fields have been demonstrated,[45,46] although there is a great gap to achieve all-electric-control magnetism. Ta/Pt/Co/Ir/Co/Pt/Ta was chosen as a reference (denoted as Co/Ir/Co, inset of Figure 1a), and the normalized magnetic hysteresis ($M-H$) loops for Ta(3)/Pt(3)/Co(0.8)/Ir(1.2)/Co(0.8)/Pt(3)/Ta(3) (in nm) can be found in Figure 1a. As expected, good PMA can be observed in the symmetric trilayer, in which the magnetic moments in both top and bottom Co layers exhibit typical antiferromagnetic coupling (AFMC). Based on the symmetrical Co/Ir/Co structure, the thickness of the bottom Co layer was increased artificially to introduce the vertical magnetic inhomogeneity. The similar IEI state can be also found in the asymmetric samples (Supporting Information (SI), Figure S1 and S2). Figure 1b presents both saturation magnetization (M_s) and effective magnetic anisotropy (K_{eff}) as functions of the bottom Co layer thickness (t_{Co}), respectively. The value of M_s is kept almost constant, and the value of K_{eff} exhibited an obvious decrease with increasing t_{Co}, from 4.56×10^6 to 2.21×10^6 erg/cm^3. Generally, the IEI strength, namely exchange coupling field (H_{ex}), can be evaluated by the shift of minor loop from vertical M-H loops. Figure 1c shows H_{ex} as a function of the Ir spacer thickness for the samples with various t_{Co}. The oscillation of H_{ex} can be found for all samples. It indicates the tunability of the IEI between ferromagnetic coupling (FMC) and antiferromagnetic coupling (AFMC), varying the period of t_{Ir} = 0.4 nm. For the samples with various t_{Co}, typical AFMC can be found in the multilayers with t_{Ir} values ranging from 1.2 to 1.4 nm. It should be noted that the maximum H_{ex} value can be tuned by changing the Ir and Co thicknesses. Therefore, magnetic properties in Co/Ir/Co trilayers can be effectively controlled by introducing vertical unbalance magnetism. Furthermore, the structural characterization was performed to assess the multilayers quality. Figure 1d presents a high-resolution, high-angle annular dark field (HAADF) scanning transmission electron microscopy

https://doi.org/10.1021/acs.nanolett.3c01192
Nano Lett. 2023, 23, 6449−6457

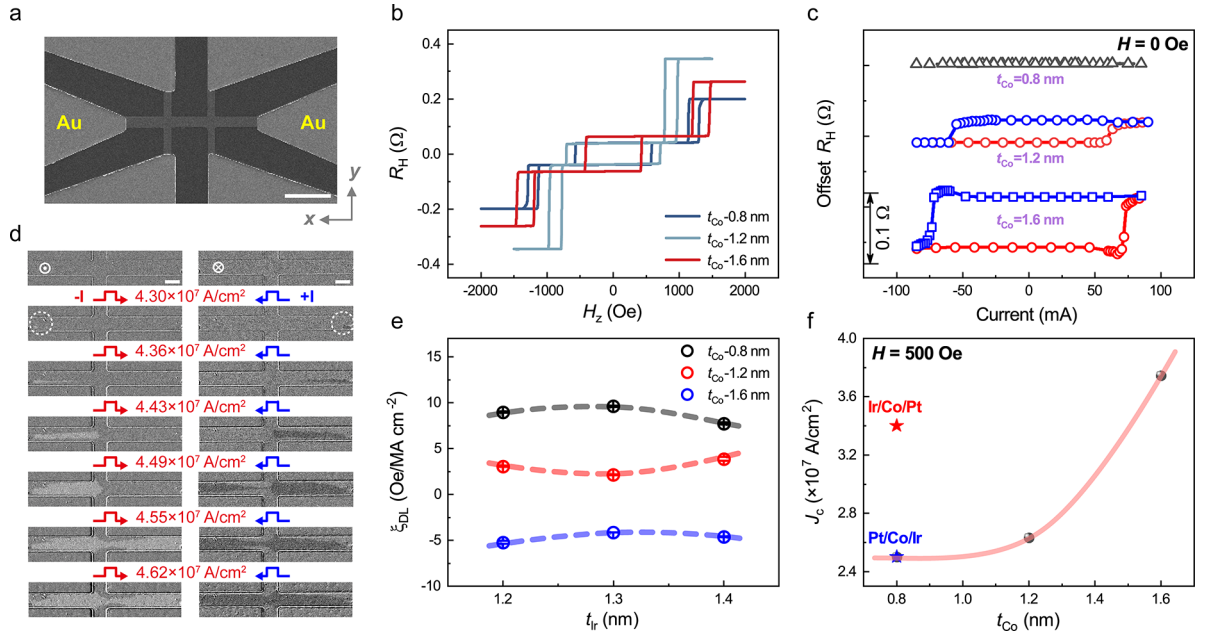

Figure 2. (a) The micrograph of Hall bar device with main channel width of 10 μm. Scale bar is 40 μ m. (b) Hall loops for the samples Co(t_{Co})/Ir/Co(0.8) trilayers (in nm), t_{Co} = 0.8, 1.2, and 1.6 nm. Scale bar is 10 μ m. (c) Current-driven magnetization switching with various t_{Co} in Co(t_{Co})/Ir/Co(0.8) trilayers (in nm) under zero external fields. (d) The current induce domain motion process in the absence of magnetic fields for Co(1.6)/Ir(1.2)/Co(0.8) trilayers (in nm). The symbols "dot within circle" and "x within circle" correspond to the up-ward and downward magnetization states, respectively. (e) The SOT efficiency (ξ_{DL}) as functions of t_{Ir} for three samples Co(0.8)/Ir/Co(0.8) (black circle), Co(1.2)/Ir/Co(0.8) (red circle), and Co(1.6)/Ir/Co(0.8) (blue circle) (in nm), respectively. (f) Critical current density (J_c) as a function of t_{Co}. The value of J_c for the Pt/Co/Ir (blue star) and Ir/Co/Pt (red star) multilayers are plotted in Figure 2f.

(STEM) image of Co(1.6)/Ir(1.4)/Co(0.8) (in nm). The atomic lattice fringes observed throughout the multilayers indicate the high-quality crystalline nature of the epitaxial multilayered structure. The two dark contrast regions originate from the continuous flat Co layers, whereas the bright contrast region located between the two Co layers is due to the thin Ir spacer. Smooth interfaces, particularly the Co/Ir and Ir/Co interfaces, can be qualitatively observed. The elemental distribution also demonstrated a clear interfacial structure using energy dispersive X-ray spectroscopy (EDS), with the maps and line scanning model shown in Figure 1e, f. Therefore, the (111) crystallographic texture can be confirmed in the sputtered Co/Ir/Co trilayers, indicating high crystallinity with a certain preferential lattice orientation.

To evaluate the magnetic transport properties, the Co/Ir/Co trilayers was patterned into a standard Hall bar device with a width of 10 μm shown in Figure 2a. Figure 2b presents anomalous Hall (AHE) loops for the sample Co(t_{Co})/Ir(1.2 nm)/Co(0.8 nm) with various t_{Co}. Multilevel switching in Hall loops can be observed under a vertical magnetic field (H_z) with increasing t_{Co}, indicating a robust AFMC between two ferromagnetic layers. However, H_{ex} showed a nonmonotonic change, suggesting the competition between various energies. The similar trend occurred in Hall resistance (R_{AHE}) via t_{Co}. Furthermore, we focus on SOT driven magnetization switching in the above samples without assistance magnetic field, as shown in Figure 2c. Surprisingly, SOT driven field-free magnetization switching can be successfully observed in the sample with t_{Co} = 1.6 nm. In constant, no magnetization switching was observed in the symmetric structure Co(0.8)/Ir/Co(0.8) (in nm) under zero fields, although a full switching behavior can be realized under various in-plane magnetic fields (SI, Figure S3a). Moreover, the partial magnetization switching can be driven without assistance magnetic fields when t_{Co} is increased to 1.2 nm. To further verify the field-free magnetization switching behavior for the imbalanced Co/Ir/Co trilayers, the domain motion process is shown in Figure 2d. In Magneto-optical Kerr effect (MOKE) image, the dark and bright domain regions correspond to the upward and downward magnetization states, respectively. For the upward state (dark region) in the main Hall channel, the critical current density (J_c) of -4.30×10^7 A/cm^2 was injected, leading to the nucleation of the reversal domain (bright region) at one side of the channel edge, marked by the white circle. With an increase in J_c to -4.36×10^7 A/cm^2, the reversal domain (bright region) occurred along the channel edge. When the J_c value was increased step by step, the white domain region continuously extended. Then, the reversal domain nearly occupied the main channel with increasing the J_c value to -4.62×10^7 A/cm^2. For the positive J_c value, a similar behavior can be observed in the main Hall channel. Both the upward and downward domain can transform each other, suggesting the nearly full magnetization switching process. Based on the MOKE results above, field-free magnetization switching in imbalanced Co/Ir/Co trilayers results from the nucleation of a new domain and its following expansion.

The harmonic measurements are performed to quantify the effective torque during the SOT driven magnetization switching process. Generally, the SOT efficiency (ξ_{DL}) is the slope of the $H_{DL}^{x} \sim J$ curve in SI Figure S4, where H_{DL}^{x} and J correspond to the damping-like field and current density, respectively. Figure 2e presents ξ_{DL} as a function of the Ir and Co thickness. The ξ_{DL} value shows a slight change with varying t_{Ir} values for the three series samples, but the sign of ξ_{DL} reverses with increasing t_{Co}. For example, the ξ_{DL} value was

https://doi.org/10.1021/acs.nanolett.3c01192
Nano Lett. 2023, 23, 6449−6457

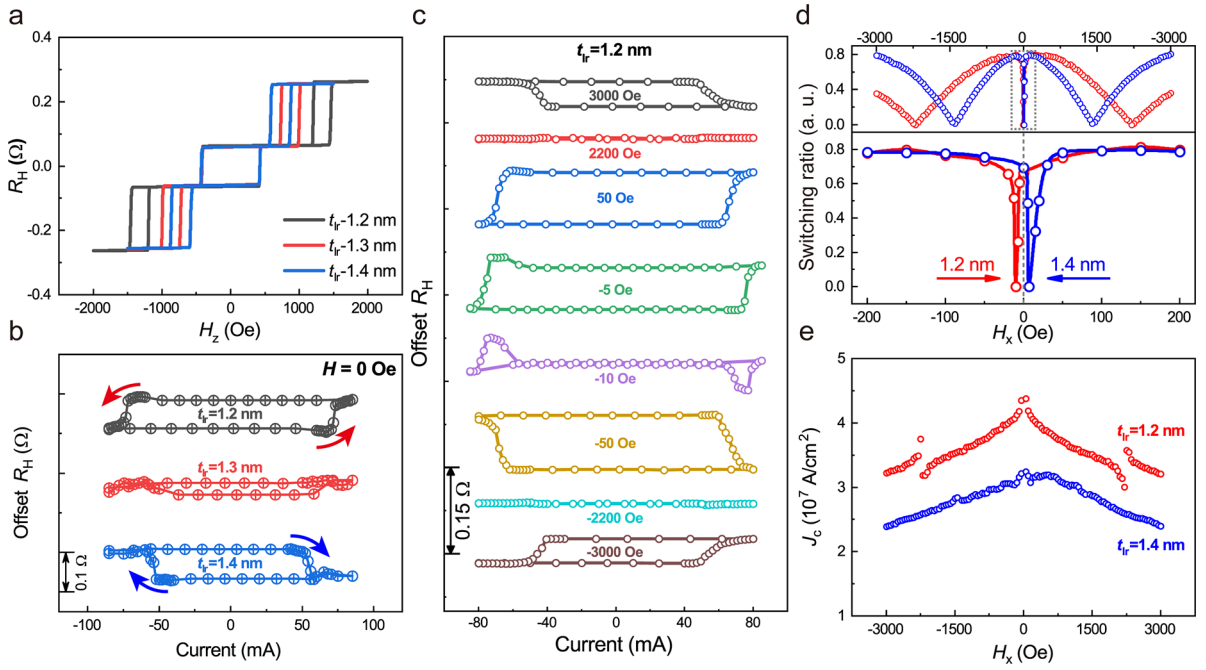

Figure 3. (a) Hall loops with various t_{Ir} in Co(1.6)/Ir(t_{Ir})/Co(0.8) (in nm), where four platforms indicate AFMC in this trilayers. (b) Current-driven magnetization switching (CDMS) with various t_{Ir} in Co(1.6)/Ir(t_{Ir})/Co(0.8) (in nm) under zero external fields. (c) Field dependence of CDMS for the sample of Co(1.6)/Ir(1.2)/Co(0.8) (in nm). (d) Switching ratio as a function of the applied magnetic fields (H_x) (red and blue circles for t_{Ir} = 1.2 and 1.4 nm). The bottom panel is an enlarged view of ±200 Oe from the top one. (e) The current density (J_c) as a function of H_x for Co(1.6)/Ir(t_{Ir})/Co(0.8) (in nm) trilayers with t_{Ir} = 1.2 and 1.4 nm.

8.96 Oe/(10^6 A cm^{-2}) for the symmetric sample Co(0.8)/Ir/Co(0.8) (in nm). Then, the ξ_{DL} value decreased to 3.07 Oe/(10^6 A cm^{-2}) in the sample with t_{Co} = 1.2 nm. With further increasing t_{Co} to 1.6 nm, a ξ_{DL} value of −5.23 Oe/(10^6 A cm^{-2}) can be observed. The reversal sign of ξ_{DL} suggests the competition between bottom and top spin generators, which is similar to the results in Pt/Co/Pt multilayers.[47] The SOT efficiency in the single Co layer was evaluated (SI, Figure S5), exhibiting positive and negative ξ_{DL} values for the Pt/Co/Ir and Ir/Co/Pt multilayers, respectively. It indicates the spin torque is dominated by the bottom Pt layer for Co(t_{Co})/Ir/Co(0.8) trilayers with t_{Co} = 0.8 nm and by the top Pt layer for the one with t_{Co} = 1.6 nm. Figure 2f presents J_c as a function of t_{Co} in the samples Co(t_{Co})/Ir/Co(0.8) (in nm) under an external magnetic field of 500 Oe. The J_c value increased with increasing t_{Co} in Co/Ir/Co trilayers, where J_c in Co(0.8)/Ir/Co(0.8) is 2.5 × 10^7 A/cm^2. Furthermore, the J_c value in the Pt/Co/Ir sample is nearly equivalent to that in the symmetric sample, which is lower than that in Ir/Co/Pt multilayers shown in Figure 2f, indicating the small SOT efficiency for the top Pt layer.

In addition, we further investigate the effect of the Ir spacer in Co/Ir/Co trilayers on deterministic magnetization switching. Figure 3a presents the Hall loops of samples with a structure of Co(1.6)/Ir(t_{Ir})/Co(0.8) (in nm). Although H_{ex} decreased significantly with increasing t_{Ir}, the AFMC was always kept in the Co/Ir/Co trilayers. Figure 3b shows the deterministic magnetization switching loops in the Co/Ir/Co trilayers with various t_{Ir}. Field-free magnetization switching can be realized successfully in the samples with t_{Ir} = 1.2 and 1.4 nm. In contrast, nearly zero deterministic switching was observed in the sample with t_{Ir} = 1.3 nm. Remarkably, the field-free switching loop was counterclockwise for the sample with t_{Ir} = 1.2 nm and clockwise for the one with t_{Ir} = 1.4 nm, clearly indicating the reversal of the magnetization switching chirality. Furthermore, switching loops with varying magnetic fields are presented in Figure 3c. A hump occurred under high current density for the partial switching, mainly due to the renucleation and annihilation of magnetic domains, consistent with the previous studies.[17] For the sample with t_{Ir} = 1.2 nm, the chirality of switching is identical, clockwise for H_x = +3000 Oe and counterclockwise for H_x = −3000 Oe. Note that the chirality reverses with a further decrease in H_x. For example, the switching is counterclockwise for H_x = +50 Oe and clockwise for H_x = −50 Oe. More importantly, there is a reversal of the switching chirality with a lower H_x= −10 Oe. The same trend was observed in the sample with t_{Ir} = 1.4 nm (SI, Figure S3c). The reversal of switching polarity can not be found in symmetric Co(0.8)/Ir/Co(0.8) trilayers. The switching ratio (η) is defined as $\eta = \Delta R_{SW}/\Delta R_{AHE}$, where ΔR_{SW} is the switching resistance and ΔR_{AHE} is the Hall resistance at zero fields. Figure 3d shows a nonlinear change in the $\eta - H_x$ curve, suggesting a strong η dependence of H_x. For example, the η value under high H_x (±1300 Oe) was found to be nearly zero for the sample with t_{Ir} = 1.4 nm. A similar case occurred for H_x = ±2200 Oe for the sample with t_{Ir} = 1.2 nm. Interestingly, the η value decreased unexpectedly to zero under very low H_x = −10 and 7 Oe for the sample with t_{Ir} = 1.2 and 1.4 nm, respectively. Figure 3e shows the current density (J_c) as a function of H_x. A J_c value of 3.1 × 10^7 A/cm^2 for field-free switching was achieved in the Co/Ir(1.4 nm)/Co trilayer. A jump of J_c observed at ±2300 Oe should be attributed to asymmetric switching induced by the edge domain walls.[48,49] Different from SOT driven magnetization switching in the double or T-type SAFs,[42−44] field-free magnetization switching in our trilayers exhibits robust chirality under applying H_x histories (SI, Figure S6b, c).

https://doi.org/10.1021/acs.nanolett.3c01192
Nano Lett. 2023, 23, 6449−6457

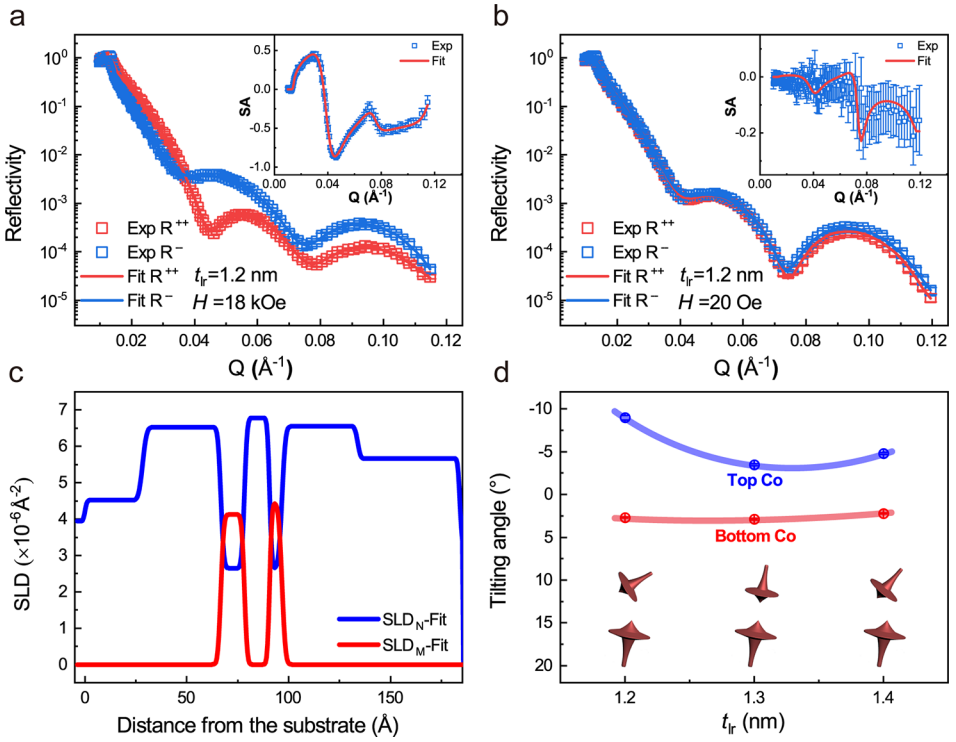

Figure 4. PNR spectra showing R^{++} (red squares) and R^{--} (blue squares) as a function of Q measured with in-plane magnetic fields of (a) 18 kOe and (b) 20 Oe for Co(1.6)/Ir(1.2)/Co(0.8) (in nm). Inset: the related spin asymmetry (SA). (c) The fitted nuclear (blue) and magnetic (red) scattering length density (SLD) profiles. (d) Tilting angle between Co magnetic moments (blue and red circles represent the top and bottom Co layers, respectively) and the normal direction of the films in Co/Ir/Co trilayers obtained from the PNR results.

Polarized neutron reflectometry (PNR) measurements were performed to verify the depth distribution of the magnetic structure. The experimental details can be found in the SI, Experimental Section and Figure S7. Generally, PNR is highly sensitive to the in-plane magnetic moment.[50−52] The tilting angles of the magnetizations can be quantitatively calibrated to confirm the spin orientation. First, an in-plane magnetic field as high as 18 kOe was applied to ensure that all of the magnetic moments lie in the film plane. The momentum-transfer (Q)-reflectivity (R^{++} or R^{--}) curves depicted in Figure 4a are strongly related to the magnetic scattering of neutrons, in which a significant difference result from spin-up or spin-down. The reflectivity curves (R^{++} or R^{--}) almost completely overlap depicted in Figure 4b, when a very low magnetic field (20 Oe) was applied because the ground state in our multilayers tended to be out-of-plane owing to the large PMA. According to the PNR result under external magnetic fields of 18 kOe, the fitted depth-resolved structural and magnetic scattering length density (SLD_N and SLD_M) are presented in Figure 4c. The multilayered structure in Co(1.6)/Ir/Co(0.8) (in nm) was confirmed by SLD results, in agreement with the STEM and EDS results shown in Figure 1. Furthermore, the insets in Figure 4a and b show the spin asymmetry (SA) as a function of Q, where the SA, defined as $(R^{++} - R^{--})/(R^{++} + R^{--})$, is sensitive to in-plane magnetization (components with $M//Q$). The weak nonzero SA indicates a small in-plane component of magnetization, confirming the canted magnetic moments for the ground state in our trilayers. Table 1 lists the in-plane components of magnetization ($M_{//}$) under various magnetic fields, where the tilting angle of the coupled magnetic moments can be exactly determined. According to the $M_{//}$ values at various H, the tilting angles were calculated to be

Table 1. In-Plane Component of Magnetizations for Co/Ir/Co Trilayers under Various Magnetic Fields

		Co(1.6)/Ir(1.2)/Co(0.8)	Co(1.6)/Ir(1.3)/Co(0.8)	Co(1.6)/Ir(1.4)/Co(0.8)	Co(0.8)/Ir(1.2)/Co(0.8)
18 kOe	Top Co	1.9 μ_B	1.9 μ_B	1.9 μ_B	1.7 μ_B
	Bottom Co	1.63 μ_B	1.85 μ_B	1.8 μ_B	1.6 μ_B
20 Oe	Top Co	−0.297 μ_B	−0.116 μ_B	−0.16 μ_B	−0.03 μ_B
	Bottom Co	0.084 μ_B	0.0935 μ_B	0.07 μ_B	0.04 μ_B

−9.0° and 2.7° for the top and bottom Co layers in Co(1.6)/Ir(1.2)/Co(0.8), respectively. The similar results can be found in Co(1.6)/Ir(t_{Ir})/Co(0.8) with various t_{Ir} (SI, Figure S8a, b). There is no doubt that the noncollinear spin texture in the ground state was confirmed in our Co/Ir/Co trilayers. The tilting angles as functions of t_{Ir} are summarized in Figure 4d. For the trilayers with AFMC, the tilting angle of the top Co layer exhibited a significant change, whereas that of the bottom Co layer remained nearly constant. More interestingly, the spin configurations transformed from noncollinear to collinear and back to noncollinear with t_{Ir} increasing from 1.2 to 1.4 nm. Note that the competition of magnetic anisotropy and interlayer exchange interaction results in the canted noncollinear spin configuration tunability. For the symmetric Co/Ir/Co trilayer, a collinear perpendicular spin configuration can be observed (SI, Figure S8c).

In conventional perpendicular SAFs, SOT driven magnetization switching can be realized under an in-plane magnetic field, which effectively breaks the chirality of domain walls. Generally, the configuration of domain wall in typical SAFs is affected by the competition of various energies, mainly

https://doi.org/10.1021/acs.nanolett.3c01192
Nano Lett. 2023, 23, 6449−6457

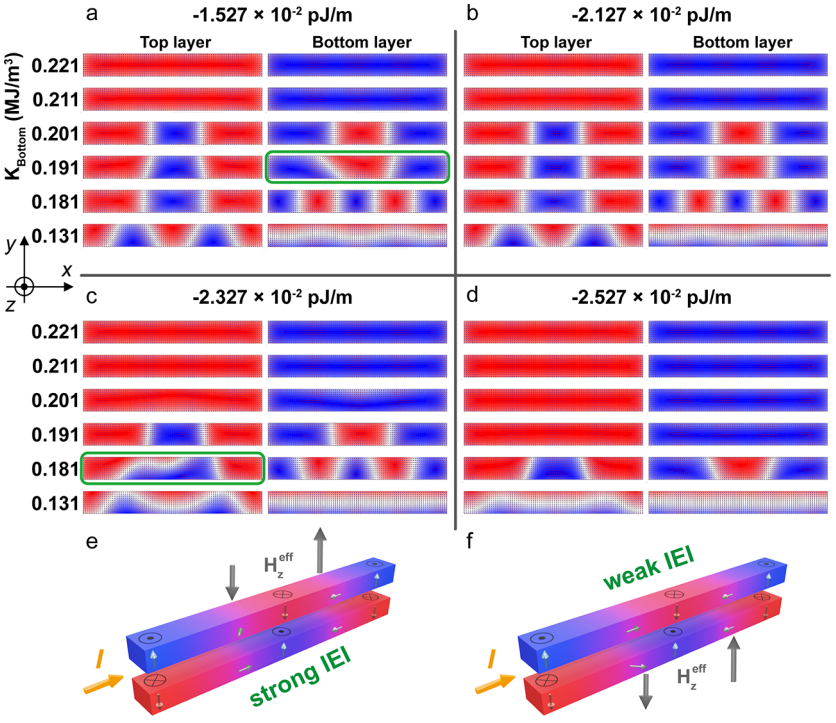

Figure 5. Micromagnetic simulation of domain wall for the trilayers with various A_{inter} and K_{bottom}. The blue and red regions represented spin point-out and point-in vertical to the plane, respectively. Domain configuration for the trilayers with various K_{bottom} at (a) $A_{inter} = -1.527 \times 10^{-2}$ pJ/m, (b) $A_{inter} = -2.127 \times 10^{-2}$ pJ/m, (c) $A_{inter} = -2.327 \times 10^{-2}$ pJ/m, (d) $A_{inter} = -2.527 \times 10^{-2}$ pJ/m, respectively. The schematic of domain walls configuration in SAFs model at (e) strong and (f) weak IEI, respectively.

including DMI, magnetic anisotropy, IEI and so on. Especially, the reduced DMI induced by different interfacial structure can result in the change of domain walls, leading to deterministic switching.[14] Here, the DMI of Co/Ir/Co was evaluated utilizing a magnetic droplet model.[53] H_{DMI} remains a constant, and its impact on asymmetric domain walls can be neglected (SI, Figure S9). Furthermore, the effect of both IEI and magnetic anisotropy on the domain wall should be paid attention, thus micromagnetic simulation was performed to deeply study the mechanism of field-free SOT driven magnetization switching. A model was proposed in which the initial state of domain wall was relaxed based on the ideal stage with both Bloch and Néel type domain walls (SI, Figure S10). In this model, the IEI strength (A_{inter}) is set from -1.327×10^{-2} to -2.527×10^{-2} pJ/m, and the anisotropy constant of the bottom Co layer (K_{bottom}) is changed from 0.131 to 0.221 MJ/m^3. Figure 5 display the typical spin configurations under various A_{inter} and K_{bottom}. For Co/Ir/Co trilayers with various A_{inter}, only a single domain can be observed when $K_{bottom} = K_{top} = 0.221$ MJ/m^3. With further decreasing K_{bottom} value, multiple-domain occurred. For the trilayers with $A_{inter} = -1.527 \times 10^{-2}$ pJ/m shown in Figure 5a, the typical Néel domain walls can be found when $K_{bottom} = 0.201$ MJ/m^3. Obviously, the mixed domain wall (Bloch-Néel type) in the bottom Co layer occurs with decreasing K_{bottom} to 0.191 MJ/m^3, leading to the asymmetric domain walls in SAFs. The similar trend can be found in the trilayer with higher A_{inter} (-2.327×10^{-2} pJ/m) and lower K_{bottom} (0.181 MJ/m^3) shown in Figure 5c. However, the asymmetric domain wall cannot be observed for the system with $A_{inter} = -2.127 \times 10^{-2}$ pJ/m (Figure 5b) and -2.527×10^{-2} pJ/m (Figure 5d). More details on the micromagnetic simulation results are shown in SI Figure S11. The asymmetric domain walls result in the net rate of domain wall expansion, which favors the reversal of the domain and leads to deterministic magnetization switching. The schematic of domain walls with various IEI is shown in Figure 5e, f based on the results of micromagnetic simulation above. Note that the asymmetric domain walls only exist in the bottom Co layer under weak IEI, and in the top Co layer under relatively strong IEI. In addition, the canted magnetization demonstrated by PNR measurements shows a strong dependence of IEI by varying the Ir spacer thickness, similar to the results of asymmetric domain walls. When the current was injected into the channel, the same direction of the total effective fields (H_z^{eff}) can be found in the layer with asymmetric domain walls. Owing to the relative orientation between the magnetization and H_z^{eff} in the layer with asymmetric domain walls, the switching polarity reverses. Therefore, the asymmetry domain wall configuration in such noncollinear canted magnets should be the main reason for all-electric-control magnetization switching.

In summary, a noncollinear canted magnetic configuration was confirmed in Co/Ir/Co trilayers with vertical magnetization gradient. Utilizing imbalance magnetism, all-electric-control magnetization switching can be successfully realized with the reversal of the switching chirality. Furthermore, the mixed chiral domain between the Néel and Bloch type originating from magnetic inhomogeneity should be the main reason for tunable SOT driven magnetization switching. Our findings in simple trilayers provide an effective pathway for the utilization of SAFs in designing low-consumption logic-in-memory.

https://doi.org/10.1021/acs.nanolett.3c01192
Nano Lett. 2023, 23, 6449−6457

■ ASSOCIATED CONTENT

Supporting Information

The Supporting Information is available free of charge at https://pubs.acs.org/doi/10.1021/acs.nanolett.3c01192.

Magnetic properties, SOT driven magnetization switching behavior, PNR measurement, characteristic of DMI, and micromagnetic simulations for Co/Ir/Co trilayers (PDF)

■ AUTHOR INFORMATION

Corresponding Authors

Jingyan Zhang − *School of Materials Science and Engineering, Beijing Advanced Innovation Center for Materials Genome Engineering, University of Science and Technology Beijing, Beijing 100083, China;* orcid.org/0000-0003-0012-6191; Email: jyzhang@ustb.edu.cn

Shouguo Wang − *School of Materials Science and Engineering, Beijing Advanced Innovation Center for Materials Genome Engineering, University of Science and Technology Beijing, Beijing 100083, China; School of Materials Science and Engineering, Anhui University, Hefei 230601, China;* Email: sgwang@ustb.edu.cn

Authors

Pengwei Dou − *School of Materials Science and Engineering, Beijing Advanced Innovation Center for Materials Genome Engineering, University of Science and Technology Beijing, Beijing 100083, China*

Yaqin Guo − *Songshan Lake Materials Laboratory, Dongguan, Guangdong 523808, China*

Tao Zhu − *Beijing National Laboratory for Condensed Matter Physics, Institute of Physics, Chinese Academy of Sciences, Beijing 100190, China*

Jia Luo − *College of Physics and Electronic Engineering, Sichuan Normal University, Chengdu 610068, China*

Guoping Zhao − *College of Physics and Electronic Engineering, Sichuan Normal University, Chengdu 610068, China;* orcid.org/0000-0002-3327-9445

He Huang − *School of Materials Science and Engineering, Beijing Advanced Innovation Center for Materials Genome Engineering, University of Science and Technology Beijing, Beijing 100083, China;* orcid.org/0000-0003-1335-3174

Guoqiang Yu − *Beijing National Laboratory for Condensed Matter Physics, Institute of Physics, Chinese Academy of Sciences, Beijing 100190, China;* orcid.org/0000-0002-7439-6920

Yunchi Zhao − *Beijing National Laboratory for Condensed Matter Physics, Institute of Physics, Chinese Academy of Sciences, Beijing 100190, China*

Jie Qi − *School of Materials Science and Engineering, Beijing Advanced Innovation Center for Materials Genome Engineering, University of Science and Technology Beijing, Beijing 100083, China;* orcid.org/0000-0002-5105-9657

Xiao Deng − *School of Materials Science and Engineering, Beijing Advanced Innovation Center for Materials Genome Engineering, University of Science and Technology Beijing, Beijing 100083, China*

Yuanbo Wang − *School of Materials Science and Engineering, Beijing Advanced Innovation Center for Materials Genome Engineering, University of Science and Technology Beijing, Beijing 100083, China*

Jialiang Li − *Beijing National Laboratory for Condensed Matter Physics, Institute of Physics, Chinese Academy of Sciences, Beijing 100190, China*

Jianxin Shen − *School of Materials Science and Engineering, Beijing Advanced Innovation Center for Materials Genome Engineering, University of Science and Technology Beijing, Beijing 100083, China*

Xinqi Zheng − *School of Materials Science and Engineering, Beijing Advanced Innovation Center for Materials Genome Engineering, University of Science and Technology Beijing, Beijing 100083, China;* orcid.org/0000-0002-1894-4910

Yanfei Wu − *School of Materials Science and Engineering, Beijing Advanced Innovation Center for Materials Genome Engineering, University of Science and Technology Beijing, Beijing 100083, China;* orcid.org/0000-0002-2081-8091

Hongxin Yang − *National Laboratory of Solid State Microstructures, School of Physics, Collaborative Innovation Center of Advanced Microstructures, Nanjing University, Nanjing 210093, China*

Baogen Shen − *Beijing National Laboratory for Condensed Matter Physics, Institute of Physics, Chinese Academy of Sciences, Beijing 100190, China;* orcid.org/0000-0003-4819-1806

Complete contact information is available at: https://pubs.acs.org/10.1021/acs.nanolett.3c01192

Author Contributions

†Pengwei Dou and Jingyan Zhang contributed equally to this paper.

Notes

The authors declare no competing financial interest.

■ ACKNOWLEDGMENTS

This work was supported by the National Key Research and Development Program of China (Grant No. 2022YFA1402602), Beijing Natural Science Foundation Key Program (Grant Nos. Z190007), and Natural Science Foundation of China (Grant Nos. 11874082, 52130103, 51971026, and 12104486).

■ REFERENCES

(1) Miron, I. M.; Garello, K.; Gaudin, G.; Zermatten, P. J.; Costache, M. V.; Auffret, S.; Bandiera, S.; Rodmacq, B.; Schuhl, A.; Gambardella, P. Perpendicular switching of a single ferromagnetic layer induced by in-plane current injection. *Nature* **2011**, *476*, 189.

(2) Liu, L. Q.; Pai, C. F.; Li, Y.; Tseng, H. W.; Ralph, D. C.; Buhrman, R. A. Spin torque switching with the giant spin Hall effect of tantalum. *Science* **2012**, *336*, 555.

(3) Nembach, H. T.; Shaw, J. M.; Weiler, M.; Jué, E.; Silva, T. J. Linear relation between Heisenberg exchange and interfacial Dzyaloshinskii−Moriya interaction in metal films. *Nat. Phys.* **2015**, *11*, 825.

(4) Qiu, X. P.; Narayanapillai, K.; Wu, Y.; Deorani, P.; Yang, D.; Noh, W.; Park, J.; Lee, K. J.; Lee, H. W.; Yang, H. Spin−orbit-torque engineering via oxygen manipulation. *Nat. Nanotechnol.* **2015**, *10*, 333.

(5) Fukami, S.; Anekawa, T.; Zhang, C.; Ohno, H. A spin−orbit torque switching scheme with collinear magnetic easy axis and current configuration. *Nat. Nanotechnol.* **2016**, *11*, 621.

(6) Cai, K. M.; Yang, M. Y.; Ju, H. L.; Wang, S. M.; Ji, Y.; Li, B. H.; Edmonds, K. W.; Sheng, Y.; Zhang, B.; Zhang, N.; Liu, S.; Zheng, H. Z.; Wang, K. Y. Electric field control of deterministic current-induced magnetization switching in a hybrid ferromagnetic/ferroelectric structure. *Nat. Mater.* **2017**, *16*, 712.

(7) Sato, N.; Xue, F.; White, R. M.; Bi, C.; Wang, S. X. Two-terminal spin−orbit torque magnetoresistive random access memory. *Nat. Electron.* **2018**, *1*, 508.
(8) Baek, S. C.; Park, K. W.; Kil, D. S.; Jang, Y.; Park, J.; Lee, K. J.; Park, B. G. Complementary logic operation based on electric-field controlled spin−orbit torques. *Nat. Electron.* **2018**, *1*, 398.
(9) Cao, Y.; Rushforth, A.; Sheng, Y.; Zheng, H. Z.; Wang, K. Y. Tuning a Binary Ferromagnet into a multistate synapse with spin−orbit-torque-induced plasticity. *Adv. Funct. Mater.* **2019**, *29*, 1808104.
(10) Razavi, A.; Wu, H.; Shao, Q. M.; Fang, C.; Dai, B. Q.; Wong, K.; Han, X. F.; Yu, G. Q.; Wang, K. L. Deterministic spin−orbit torque switching by a light-metal insertion. *Nano Lett.* **2020**, *20*, 3703.
(11) Liu, L. Q.; Moriyama, T.; Ralph, D. C.; Buhrman, R. A. Spin-torque ferromagnetic resonance induced by the spin Hall effect. *Phys. Rev. Lett.* **2011**, *106*, 036601.
(12) He, P.; Qiu, X. P.; Zhang, V. L.; Wu, Y.; Kuok, M. H.; Yang, H. Continuous tuning of the magnitude and direction of spin-orbit torque using bilayer heavy metals. *Adv. Electron. Mater.* **2016**, *2*, 1600210.
(13) Yu, G. Q.; Upadhyaya, P.; Fan, Y. B.; Alzate, J. G.; Jiang, W. J.; Wong, K. L.; Takei, S.; Bender, S. A.; Chang, L. T.; Jiang, Y.; Lang, M.; Tang, J. S.; Wang, Y.; Tserkovnyak, Y.; Amiri, P. K.; Wang, K. L. Switching of perpendicular magnetization by spin−orbit torques in the absence of external magnetic fields. *Nat. Nanotechnol.* **2014**, *9*, 548.
(14) Chen, R. Y.; Cui, Q. R.; Liao, L. Y.; Zhu, Y. M.; Zhang, R. Q.; Bai, H.; Zhou, Y. J.; Xing, G. Z.; Pan, F.; Yang, H. X.; Song, C. Reducing Dzyaloshinskii-Moriya interaction and field-free spin-orbit torque switching in synthetic antiferromagnets. *Nat. Commun.* **2021**, *12*, 3113.
(15) Cui, B. S.; Wu, H.; Li, D.; Razavi, S. A.; Wu, D.; Wong, K. L.; Chang, M. X.; Gao, M. Z.; Zuo, Y. L.; Xi, L.; Wang, K. L. Field-free spin−orbit torque switching of perpendicular magnetization by the Rashba interface. *ACS Appl. Mater. Interfaces* **2019**, *11*, 39369.
(16) Zheng, Z.; Zhang, Y.; Lopez-Dominguez, V.; Sanchez-Tejerina, L.; Shi, J.; Feng, X.; Chen, L.; Wang, Z.; Zhang, Z.; Zhang, K.; et al. Field-free spin-orbit torque-induced switching of perpendicular magnetization in a ferrimagnetic layer with a vertical composition gradient. *Nat. Commun.* **2021**, *12*, 4555.
(17) Liu, L.; Song, Y. H.; Zhao, X. T.; Liu, W.; Zhang, Z. D. Full-scale field-free spin-orbit torque switching in HoCo structure with a vertical composition gradient. *Adv. Funct. Mater.* **2022**, *32*, 2200328.
(18) Liu, L.; Zhou, C. H.; Zhao, T. Y.; Yao, B. Q.; Zhou, J.; Shu, X. Y.; Chen, S. H.; Shi, S.; Xi, S. B.; Lan, D.; et al. Current-induced self-switching of perpendicular magnetization in CoPt single layer. *Nat. Commun.* **2022**, *13*, 3539.
(19) Oh, Y.-W.; Chris Baek, S.-h.; Kim, Y. M.; Lee, H. Y.; Lee, K.-D.; Yang, C.-G.; Park, E.-S.; Lee, K.-S.; Kim, K.-W.; Go, G.; et al. Field-free switching of perpendicular magnetization through spin−orbit torque in antiferromagnet/ferromagnet/oxide structures. *Nat. Nanotechnol.* **2016**, *11*, 878.
(20) Lau, Y. C.; Betto, D.; Rode, K.; Coey, J. M. D.; Stamenov, P. Spin−orbit torque switching without an external field using interlayer exchange coupling. *Nat. Nanotechnol.* **2016**, *11*, 758.
(21) Yun, J. J.; Bai, Q. N.; Yan, Z.; Chang, M. X.; Mao, J.; Zuo, Y. L.; Yang, D. Z.; Xi, L.; Xue, D. S. Tailoring Multilevel-Stable Remanence States in exchange-biased system through spin-orbit torque. *Adv. Funct. Mater.* **2020**, *30*, 1909092.
(22) Zhu, W. K.; Lin, H. L.; Yan, F. G.; Hu, C.; Wang, Z.; Zhao, L. X.; Deng, Y. C.; Kudrynskyi, Z. R.; Zhou, T.; Kovalyuk, Z. D.; Zheng, Y. H.; Patanè, A.; Žutić, I.; Li, S. S.; Zheng, H. Z.; Wang, K. Y. Large tunneling magnetoresistance in van der Waals ferromagnet/semiconductor heterojunctions. *Adv. Mater.* **2021**, *33*, 2104658.
(23) Zhu, W. K.; Xie, S. H.; Lin, H. L.; Zhang, G. J.; Wu, H.; Hu, T. G.; Wang, Z.; Zhang, X. M.; Xu, J. H.; Wang, Y. J.; Zheng, Y. H.; Yan, F. G.; Zhang, J.; Zhao, L. X.; Patané, A.; Zhang, J.; Chang, H. X.; Wang, K. Y. Large room-temperature magnetoresistance in van der Waals ferromagnet/semiconductor junctions. *Chin. Phys. Lett.* **2022**, *39*, 128501.
(24) Kao, I. H.; Muzzio, R.; Zhang, H. T.; Zhu, M. L.; Gobbo, J.; Yuan, S.; Weber, D.; Rao, R.; Li, J. H.; Edgar, J. H.; Goldberger, J. E.; Yan, J. Q.; Mandrus, D. G.; Hwang, J.; Cheng, R.; Katoch, J.; Singh, S. Deterministic switching of a perpendicularly polarized magnet using unconventional spin−orbit torques in WTe_2. *Nat. Mater.* **2022**, *21*, 1029.
(25) Mahendra, D. C.; Shao, D. F.; Hou, V. D.H.; Vailionis, A.; Quarterman, P.; Habiboglu, A.; Venuti, M. B.; Xue, F.; Huang, Y. L.; Lee, C. M.; et al. Observation of anti-damping spin−orbit torques generated by in-plane and out-of-plane spin polarizations in $MnPd_3$. *Nat. Mater.* **2023**, *22*, 591.
(26) Deng, Y. C.; Liu, X. H.; Chen, Y. Y.; Du, Z. Z.; Jiang, N.; Shen, C.; Zhang, E.; Zheng, H. Z.; Lu, H. Z.; Wang, K. Y. All-electrical switching of a topological non-collinear antiferromagnet at room temperature. *Natl. Sci. Rev.* **2023**, *10*, nwac154.
(27) Mishra, R.; Yu, J. W.; Qiu, X. P.; Motapothula, M.; Venkatesan, T.; Yang, H. Anomalous current-induced spin torques in ferrimagnets near compensation. *Phys. Rev. Lett.* **2017**, *118*, 167201.
(28) Yu, J.; Bang, D.; Mishra, R.; Ramaswamy, R.; Oh, J. H.; Park, H.-J.; Jeong, Y.; Van Thach, P.; Lee, D.-K.; Go, G.; et al. Long spin coherence length and bulk-like spin−orbit torque in ferrimagnetic multilayers. *Nat. Mater.* **2019**, *18*, 29.
(29) Wu, H.; Xu, Y.; Deng, P.; Pan, Q.; Razavi, S. A.; Wong, K.; Huang, L.; Dai, B.; Shao, Q.; Yu, G.; et al. Spin-orbit torque switching of a nearly compensated ferrimagnet by topological surface states. *Adv. Mater.* **2019**, *31*, 1901681.
(30) Wu, H.; Groß, F.; Dai, B. Q.; Lujan, D.; Razavi, S. A.; Zhang, P.; Liu, Y. X.; Sobotkiewich, K.; Förster, J.; Weigand, M.; Schütz, G.; Li, X. Q.; Gräfe, J.; Wang, K. L. Ferrimagnetic skyrmions in topological insulator/ferrimagnet heterostructures. *Adv. Mater.* **2020**, *32*, 2003380.
(31) Liu, J. H.; Xu, T.; Feng, H. M.; Zhao, L.; Tang, J. S.; Fang, L.; Jiang, W. J. Compensated ferrimagnet based artificial synapse and neuron for ultrafast neuromorphic computing. *Adv. Funct. Mater.* **2022**, *32*, 2107870.
(32) Wadley, P.; Howells, B.; Železný, J.; Andrews, C.; Hills, V.; Campion, R. P.; Novák, V.; Olejník, K.; Maccherozzi, F.; Dhesi, S. S.; Martin, S. Y.; Wagner, T.; Wunderlich, J.; Freimuth, F.; Mokrousov, Y.; Kuneš, J.; Chauhan, J. S.; Grzybowski, M. J.; Rushforth, A. W.; Edmonds, K. W.; Gallagher, B. L.; Jungwirth, T. Electrical switching of an antiferromagnet. *Science* **2016**, *351*, 587.
(33) Jungwirth, T.; Marti, X.; Wadley, P.; Wunderlich, J. Antiferromagnetic spintronics. *Nat. Nanotechnol.* **2016**, *11*, 231.
(34) Jin, C. D.; Song, C. K.; Wang, J. B.; Liu, Q. F. Dynamics of antiferromagnetic skyrmion driven by the spin Hall effect. *Appl. Phys. Lett.* **2016**, *109*, 182404.
(35) Shen, L. C.; Xia, J.; Zhao, G. P.; Zhang, X. C.; Ezawa, M.; Tretiakov, O. A.; Liu, X. X.; Zhou, Y. Dynamics of the antiferromagnetic skyrmion induced by a magnetic anisotropy gradient. *Phys. Rev. B* **2018**, *98*, 134448.
(36) Göbel, B.; Mook, A.; Henk, J.; Mertig, I. Antiferromagnetic skyrmion crystals: Generation, topological Hall, and topological spin Hall effect. *Phys. Rev. B* **2017**, *96*, 060406.
(37) Marti, X.; Fina, I.; Frontera, C.; Liu, J.; Wadley, P.; He, Q.; Paull, R. J.; Clarkson, J. D.; Kudrnovsky, J.; Turek, I.; Kunes, J.; Yi, D.; Chu, J. H.; Nelson, C. T.; You, L.; Arenholz, E.; Salahuddin, S.; Fontcuberta, J.; Jungwirth, T.; Ramesh, R. Room-temperature antiferromagnetic memory resistor. *Nat. Mater.* **2014**, *13*, 367.
(38) Yan, H.; Feng, Z.; Shang, S.; Wang, X.; Hu, Z.; Wang, J.; Zhu, Z.; Wang, H.; Chen, Z.; Hua, H.; Lu, W.; Wang, J.; Qin, P.; Guo, H.; Zhou, X.; Leng, Z.; Liu, Z.; Jiang, C.; Coey, M.; Liu, Z. Q. A piezoelectric, strain-controlled antiferromagnetic memory insensitive to magnetic fields. *Nat. Nanotechnol.* **2019**, *14*, 131.
(39) Bodnar, S. Y.; Smejkal, L.; Turek, I.; Jungwirth, T.; Gomonay, O.; Sinova, J.; Sapozhnik, A. A.; Elmers, H.-J.; Klaui, M.; Jourdan, M. Writing and reading antiferromagnetic Mn_2Au by Néel spin-orbit torques and large anisotropic magnetoresistance. *Nat. Commun.* **2018**, *9*, 348.

https://doi.org/10.1021/acs.nanolett.3c01192
Nano Lett. 2023, 23, 6449−6457

(40) Yang, S. H.; Ryu, K. S.; Parkin, S. S. P. Domain-wall velocities of up to 750 m s^{-1} driven by exchange-coupling torque in synthetic antiferromagnets. *Nat. Nanotechnol.* **2015**, *10*, 221.
(41) Duine, R. A.; Lee, K. J.; Parkin, S. S. P.; Stiles, M. D. Synthetic antiferromagnetic spintronics. *Nat. Phys.* **2018**, *14*, 217.
(42) Wei, J. W.; Wang, X.; Cui, B. S.; Guo, C. Y.; Xu, H. J.; Guang, Y.; Wang, Y. Q.; Luo, X. M.; Wan, C. H.; Feng, J. F.; Wei, H. X.; Yin, G.; Han, X. F.; Yu, G. Q. Field-free spin−orbit torque switching in perpendicularly magnetized synthetic antiferromagnets. *Adv. Funct. Mater.* **2022**, *32*, 2109455.
(43) Wang, X.; Wan, C. H.; Kong, W. J.; Zhang, X.; Xing, Y. W.; Fang, C.; Tao, B. S.; Yang, W. L.; Huang, L.; Wu, H.; Irfan, M.; Han, X. F. Field-free programmable spin logics via chirality-reversible spin−orbit torque switching. *Adv. Mater.* **2018**, *30*, 1801318.
(44) Kong, W. J.; Wan, C. H.; Wang, X.; Tao, B. S.; Huang, L.; Fang, C.; Guo, C. Y.; Guang, Y.; Irfan, M.; Han, X. F. Spin−orbit torque switching in a T-type magnetic configuration with current orthogonal to easy axes. *Nat. Commun.* **2019**, *10*, 233.
(45) Ma, Q. L.; Li, Y. F.; Choi, Y. S.; Chen, W. C.; Han, S. J.; Chien, C. L. Spin orbit torque switching of synthetic Co/Ir/Co trilayers with perpendicular anisotropy and tunable interlayer coupling. *Appl. Phys. Lett.* **2020**, *117*, 172403.
(46) Dohi, T.; DuttaGupta, S.; Fukami, S.; Ohno, H. Formation and current-induced motion of synthetic antiferromagnetic skyrmion bubbles. *Nat. Commun.* **2019**, *10*, 5153.
(47) Cao, Y.; Sheng, Y.; Edmonds, K. W.; Ji, Y.; Zheng, H. Z.; Wang, K. Y. Deterministic magnetization switching using lateral spin−orbit torque. *Adv. Mater.* **2020**, *32*, 1907929.
(48) Zhao, X. T.; Liu, W.; Li, S. K.; Wang, T. T.; Liu, L.; Song, Y. H.; Ma, S.; Zhao, X. G.; Zhang, Z. D. Asymmetric current-driven switching of synthetic antiferromagnets with Pt insert layers. *Nanoscale* **2018**, *10*, 7612.
(49) Wang, K.; Qian, L. J.; Ying, S. C.; Xiao, G. Spin-orbit torque switching of chiral magnetization across a synthetic antiferromagnet. *Commun. Phys.* **2021**, *4*, 10.
(50) Ankner, J. F.; Felcher, G. P. Polarized-neutron reflectometry. *J. Magn. Magn. Mater.* **1999**, *200*, 741.
(51) Zhu, T.; Yang, Y.; Yu, R. C.; Ambaye, H.; Lauter, V.; Xiao, J. Q. The study of perpendicular magnetic anisotropy in CoFeB sandwiched by MgO and tantalum layers using polarized neutron reflectometry. *Appl. Phys. Lett.* **2012**, *100*, 202406.
(52) Zhang, J. Y.; Zhang, Y.; Gao, Y.; Zhao, G. P.; Qiu, L.; Wang, K. Y.; Dou, P. W.; Peng, W. L.; Zhuang, Y.; Wu, Y. F.; Yu, G. Q.; Zhu, Z. Z.; Zhao, Y. C.; Guo, Y. Q.; Zhu, T.; Cai, J. W.; Shen, B. G.; Wang, S. G. Magnetic skyrmions in a Hall balance with interfacial canted magnetizations. *Adv. Mater.* **2020**, *32*, 1907452.
(53) Kim, S.; Jang, P. H.; Kim, D. H.; Ishibashi, M.; Taniguchi, T.; Moriyama, T.; Kim, K. J.; Lee, K. J.; Ono, T. Magnetic droplet nucleation with a homochiral Néel domain wall. *Phys. Rev. B* **2017**, *95*, 220402.

https://doi.org/10.1021/acs.nanolett.3c01192
Nano Lett. 2023, 23, 6449−6457